Kinetic oxidation model including the transient regime for a single crystal nickel-based superalloy over the temperature range 750–1300 °C

Thomas Perez, Daniel Monceau, Clara Desgranges

Kinetic oxidation model including the transient regime for a single crystal nickel-based superalloy over the temperature range 750-1300 ° C

Thomas Perez, Daniel Monceau, Clara Desgranges

PII: S0010-938X(22)00403-6

DOI: https://doi.org/10.1016/j.corsci.2022.110485

Reference: CS110485

To appear in: *Corrosion Science*

Received date: 15 February 2022
Revised date: 30 June 2022
Accepted date: 11 July 2022

Please cite this article as: Thomas Perez, Daniel Monceau and Clara Desgranges, Kinetic oxidation model including the transient regime for a single crystal nickel-based superalloy over the temperature range 750-1300 ° C, *Corrosion Science,* (2022) doi:https://doi.org/10.1016/j.corsci.2022.110485

Kinetic oxidation model including the transient regime for a single crystal nickel-based superalloy over the temperature range 750-1300 ° C

Thomas Perez [a], Daniel Monceau [a], Clara Desgranges [b]

[a] CIRIMAT, CNRS-INPT-UPS, ENSIACET, 4 allée Emile Monso, BP 44362, 31030 Toulouse Cedex 4, France

[b] Safran Tech, Rue des Jeunes Bois, Châteaufort, CS 80112, 78772 Magny-Les-Hameaux, France

Corresponding author: thomas.perez@toulouse-inp.fr

Abstract

The oxidation behavior of the Ni-base single-crystal superalloy AM1 was investigated over the temperature range 750 to 1300°C. The use of stepwise multi-temperature thermogravimetric analysis (SMT-TGA) showed the presence of a transient regime. This transient regime can be modeled by the initial formation of a fast-growing mixed oxide and then by the formation of α-alumina gradually covering the metal/oxide interface. This model helps to determine the time required for AM1 alloy to be out of the transient regime. Then, the model makes it possible to predict any oxidation kinetics of the AM1 superalloy for the entire temperature range studied.

Keywords
AM1, superalloy, high temperature oxidation, transient oxidation, oxidation kinetics

Introduction

Alloy AM1[1,2] is a first-generation monocrystalline superalloy. It is used for high-pressure turbine blades in aeronautical gas turbines. For this particular application, it is protected by a NiPtAl coating and by a thermal barrier deposited by EB PVD [3]. However, the inside of the blades, subjected to lower temperatures, may not be coated. Alloy AM1 can also be used without a protective coating in other components for lower temperatures. A recent study [4] showed that the uncoated AM1 alloy under cyclic oxidation condition at 1100°C in laboratory air has an excellent oxidation resistance, equivalent or even superior to this same superalloy with a NiPtAl coating. But this may not be the case at lower temperatures. Less protective oxides may be formed at lower temperatures. Therefore, this study will focus on the isothermal oxidation behavior of uncoated AM1 alloy in a larger temperature range than previously reported.

In the literature, few studies report the oxidation behavior of uncoated AM1 [4-6] and only at the highest temperatures of use. Isothermal oxidations are reported only at 1100°C [5]. Cyclic oxidation data for this alloy are reported only at 1100°C [4] and 1150°C [6]. Over these temperatures, gamma prime precipitates volume fraction is too low to ensure good creep

resistance properties. After oxidation at 1100-1150°C, the samples showed similar oxide scale microstructures. The typical oxide scale is composed of a layer of α-Al_2O_3 at the metal/oxide interface, surmounted by a spinel layer with the presence of precipitates rich in Ti and Ta at the interface between the two layers or in the spinel layer. Other single-crystal nickel-based superalloys, for example, the René N5 alloy in isothermal oxidation [7] and the CMSX-4 alloy in cyclic oxidation [8], form an oxide scale similar to that observed on the AM1 alloy at 1100°C.

At lower temperature, the formation of a protective alumina scale may be not achieved. At 950°C, the oxide scale formed on CMSX-4 alloy after 100h is composed of α-alumina, spinel and rutile [9] as at higher temperatures, but it is not the case at lower temperature. Indeed, Sudbrack et al. [10] studied the oxidation of CMSX-4 alloy and LDS-1101 alloy at 815°C with different surface preparation. The isothermal oxidation of LDS-1101 alloy at 815°C leads to the formation of an α-alumina layer close to the metal/oxide interface and θ-Al_2O_3 close to the oxide/gas interface. At 815°C, the oxide scale grown on CMSX-4 alloy is composed of alumina, chromia, spinel and Ta, Cr rich oxide, after 444 cycles of 1 h. Hence, the literature on similar superalloys than AM1 indicates that there are two possible scenarios for the oxidation of this alloy at lower temperatures, which should both lead to a significant transient regime.

The quantification of the oxidation kinetics is important since it allows to predict the depletion of the γ' precipitates and thus the influence of oxidation on the mechanical properties of the part [11-13]. The oxidation atmosphere and the growth mechanism of the oxide layer could also influence the creep rate [14]. Only few studies had proposed kinetics oxidation models involving a transient regime due to a change with time in the nature of the external protective oxide. To model the isothermal oxidation of Ni-Cr-Al alloys, with a transient regime, Nijdam et al. used a cubic and linear laws until a transition time and then a simple parabolic law [15]. For Fe-Cr and Fe-Ni-Cr alloys under Ar-CO_2 [16], Gheno et al. had modeled a change of oxide regime with a transition from a parabolic oxidation (formation of chromia) to a breakaway (formation of iron oxide). This change of regime was modeled by considering progressive covering of the surface by precipitates of non-protective iron oxide. The surface occupied by the precipitates experienced a rapid growth of its oxide layer, while the surface without precipitates remained with the growth rate of chromia.

In the present paper, the oxidation behavior of AM1 was studied using the stepwise multi-temperature thermogravimetric analyses (SMT-TGA), a method particularly useful to determine oxidation behavior over in a large temperature range with a single sample. Complementary isothermal thermogravimetric analyses were also performed to deepen the understanding of the nature of the transient regime. The nature of the oxides formed on AM1 at different temperatures has been investigated by SEM, EBSD and XRD. A model is proposed to simulate the oxidation kinetics of AM1 over the entire temperature range studied, and including the transient regime.

Material and methods

A cylinder of AM1 alloy was provided by Safran Aircraft Engine. The chemical composition of the alloy is presented in Table 1. The alloy was analyzed by Glow Discharge Mass Spectrometry for impurities and X-ray fluorescence for other elements.

Specimens with dimensions of 10 × 10 × 1 or 2 mm were cut from a plain cylinder and ground to P600 grit surface finish. Each coupon was degreased in acetone and alcohol, then weighed before the oxidation test. The oxidation tests were performed in SETARAM TAG24 S thermobalances. The samples were oxidized in a flow of synthetic air of 20 ml/min (1.2 l/h). All the heating rates and initial cooling rates were 1°C/s. Two different oxidation tests were carried out. The first type was a classic isothermal oxidation and the second one was a stepwise multi-temperature thermogravimetric analysis (SMT-TGA). This last type of test consists of multiple steps and temperature dwells. The duration of the different dwells are appropriately chosen to obtain the best signal-to-noise ratio, with approximately the same mass gain at each dwell. During the test, the data points are recorded every 10 s.

SMT-TGA makes use of a single sample to measure the oxidation kinetics at different temperatures, instead of using several samples in different isothermal tests. This procedure reduces the experimental variations coming from the sample geometry or microstructure. The main advantage of SMT-TGA is the gain in time and in matter when alloy availability is limited, for example during the alloy development process. However, a history effect on the single sample can exist between the different temperatures tested. This can affect the mass gains and then the estimation of kinetics parameters. Indeed, the oxidation rate depends on the microstructure of the oxide layer formed, e.g., [17], and the microstructure depends on the thermal history of the sample. Also, the nature of the oxide scale can change during oxidation time [16]. In order to investigate a possible history effect, the same temperature is used for two different dwells in the SMT-TGA, one during the rising steps of temperature and the other one during the cooling steps. The history effect can then be evidenced by comparing the kinetics parameters measured during the two different dwells at the same temperature. If the oxidation kinetics is the same during the two dwells, one may conclude that there is no history effect. Whereas if the oxidation rates are different for the two dwells, a history effect is evidenced. SMT-TGA is a relatively fast way to obtain the oxidation behavior of alloys over a large temperature range. Hence, the aim is to build an entire Arrhenius plot of the parabolic rate constant with a single sample. To investigate the reliability of the SMT-TGA in the case of the AM1 alloy, nine classic isothermal tests of TGA at different temperatures between 800°C and 1200°C were also carried out.

After each oxidation test, the oxide scale was analyzed with X-ray diffraction on a BrukerD8 GIXR using Cu-Kα radiation, with a step size of 0.02°, an angle of incidence of 10°, a scan step time of 2 s in the 2θ range from 15° to 80°. Cross-section characterizations were conducted on a SEM FEI Quanta 450 equipped with an EDS detector Bruker Quantax (SDD). EBSD analyses were performed on a scanning electron microscope JEOL JSM-7100 equipped with an EBSD camera NordlyNano. To avoid any spallation of the oxide scale during polishing of the cross-sections, the oxidized samples were coated with a thin layer of silver and then with an electroplated copper layer.

Results

Stepwise multi-temperature thermogravimetric analysis (SMT-TGA)

A stepwise multi-temperature thermogravimetric analysis [18-23] (Fig. 1a) was realized to evaluate the oxidation behavior of AM1. This thermogravimetric analysis is composed of 12

steps chaining temperature dwells between 750 and 1300°C in order to obtain the evolution of mass gain of the sample during each dwell. The whole SMT-TGA was 320 h long. The details of the chain of (time, temperature) dwells for this test are gathered in Table 2. In this experiment, ten of the twelve temperature dwells were analyzed.

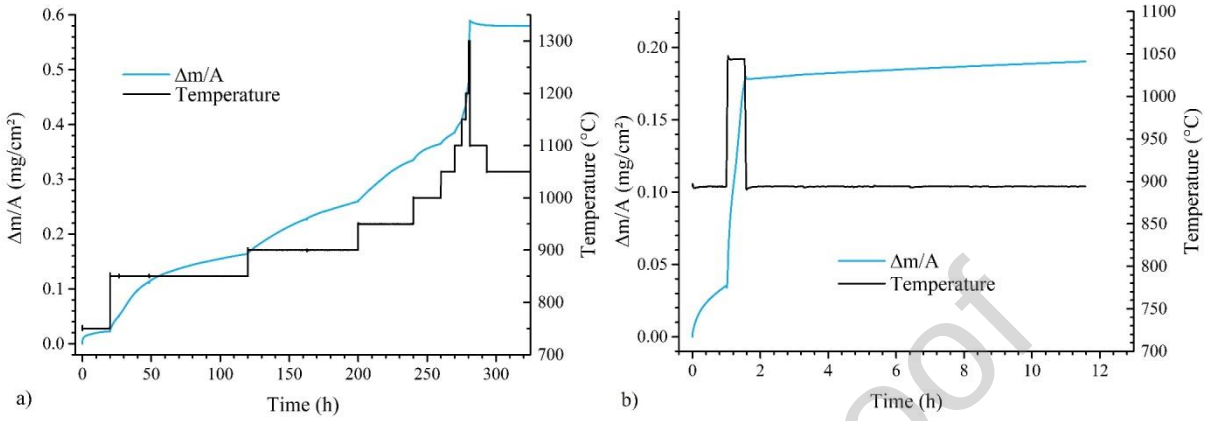

Fig. 1. Thermal cycles and evolution of mass gain as a function of time, a) SMT-TGA and b) specific test at 900-1050-900°C.

Indeed, spallation of a part of the oxide scale occurred during the last two temperature dwells. This spallation during these last two stages prevented the precise determination of the kinetic parameters. Therefore, another oxidation test was realized, with only three steps, a step at 900°C (1 h) then a step at 1050°C (0.5 h) and again a step at 900°C (10 h) in order to investigate if a "history effect" was present on our sample.

To determine the parabolic constant of oxidation k_p on each step, the complete parabolic law (Eq1) was used [19].

$$t = A + B \times m + C \times m^2 \quad \text{with} \quad k_p = \frac{1}{C} \qquad \text{Eq1}$$

Where t is the time and m is the mass gain per unit surface area. The parameters A, B and C were adjusted to fit the evolution of mass gain on each temperature step. Local fitting of this same complete parabolic law was applied in a fitting window translated over the entire temperature step, as detailed in [19] and shown in Fig. 2. In this case, the time evolution of the parameter k_p was recorded to represent the oxidation kinetics of this particular dwell.

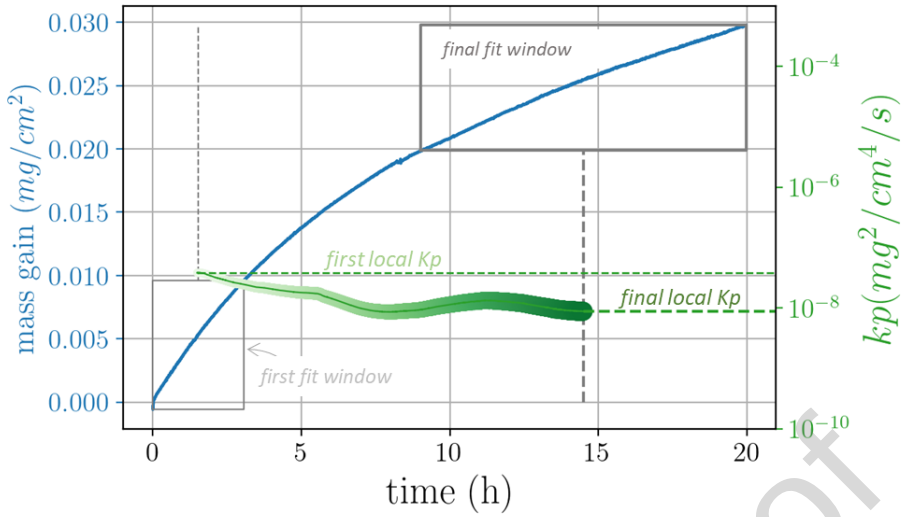

Fig. 2. Evaluation of the instantaneous parabolic rate constant k_p as a function of time using the adjustment of the mass gain curve with a complete parabolic law in a gliding window [19]. Application to the dwell at 1000°C of the SMT-TGA experiment.

As explained in [19], it is important to use the complete parabolic law (Eq1) for the determination of the parabolic rate constant when the parabolic regime is preceded by a transient regime. In the case of SMT-TGA, the mass gain at the beginning of a dwell corresponds to an oxide scale formed at a different temperature with different oxidation kinetics, therefore it is mandatory to use a kinetic model able to deal with this change in oxidation regime.

The same procedure had been used to evaluate the parabolic constant k_p from the mass gain curve on each dwell of the SMT-TGA experiment. As shown before in Fig.2 for the dwell at 1000°C, the value of k_p determined at the beginning of the dwell at 950°C is one order of magnitude greater than at the end of the dwell. For the next six dwells in the SMT-TGA experiment between 1000°C en 1300°C, the difference between the initial and final k_p values is significantly smaller. This is the sign of the existence of a transitory regime in the oxidation rate that ends at the beginning of the stage at 1000°C.

The values of k_p obtained from the analysis of the whole SMT-TGA experiment are plotted in an Arrhenius diagram in Fig. 3. The k_p values corresponding to the growth of α-Al_2O_3 on β-NiAl measured by Brumm and Grabke [24] and the k_p values of Cr_2O_3 formed on Ni-30Cr from Huang et al. [25] are also reported in the same plot as plain lines.

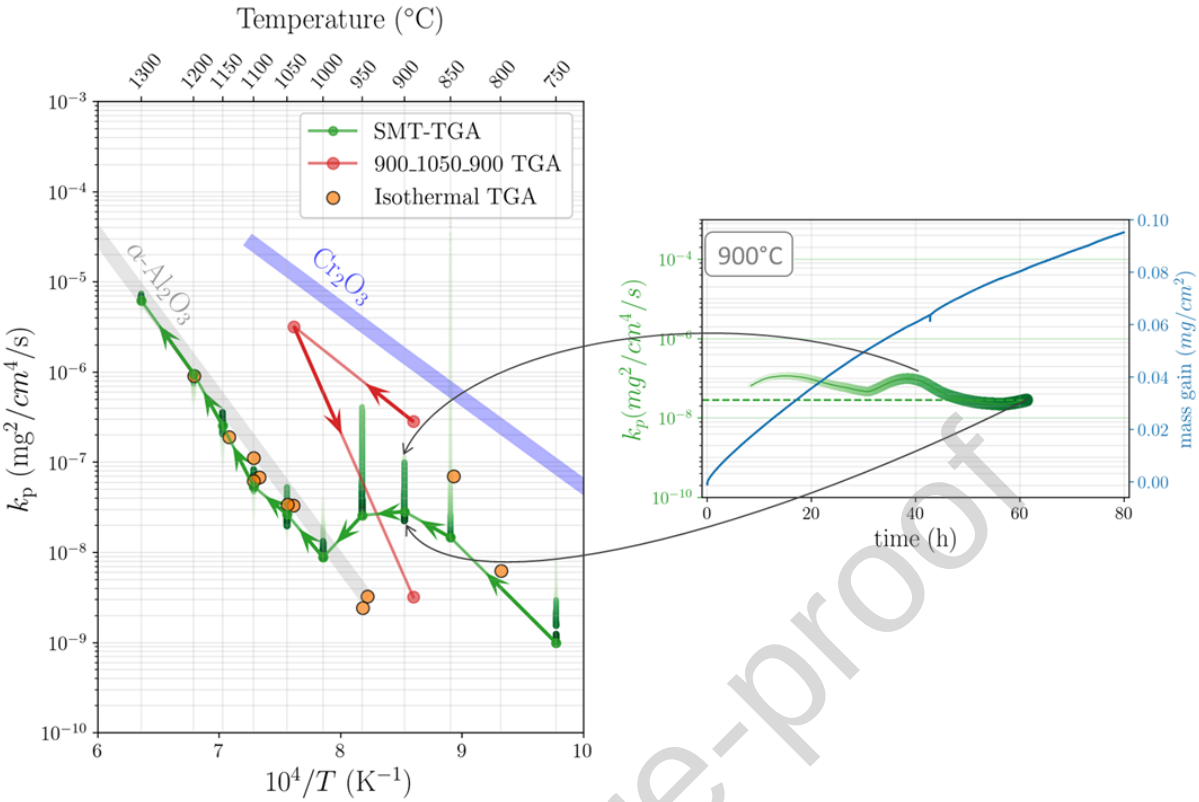

Fig.3. Arrhenius plot of the parabolic rate constant k_p determined for the AM1 alloy with the three kinds of TGA experiments (SMT-TGA, 900-1050-900°C and isothermal). For the dwells at the lowest temperatures of the SMT-TGA experiment, the evolution of the parabolic constant k_p with time is shown (short times in light green to long times in dark green). The final instantaneous k_p estimated at the end of each temperature dwell are linked together with arrows following the temperature dwell sequence for SMT-TGA. The same was done for the 900-1050-900 experiment. The kp reported as orange dots correspond to isothermal TGA experiments and are also the final instantaneous k_p. Lines of the Arrhenius laws for α-Al_2O_3 growth on NiAl [24], and for Cr_2O_3 growth on Ni-30Cr alloy [25] are shown for comparison.

Over the temperature range 1050 to 1300°C, the values of the parabolic constant k_p determined for the AM1 alloy with the SMT-TGA follow an Arrhenius law. This law is very close to the one reported for α-Al_2O_3 formed on NiAl [24]. Between 750°C and 950°C, the k_p values determined for the AM1 alloy seem also to follow an Arrhenius law (even if the k_p decreases with time). As seen in the Arrhenius plot, this second law lies somewhere between that reported in the literature for α-Al_2O_3 formed on NiAl [24] and that reported for Cr_2O_3 formed on Ni-30Cr alloy [25]. Besides, over the temperature range 950 to 1050°C, it is worth noting that the k_p determined by the SMT-TGA decreases with the increasing temperature. This evolution results from the transition between the two different Arrhenius laws. This kind of abnormal evolution of the k_p constant with the temperature has already been reported for NiCoCrAlY coating [26], but in this case, the k_p values between the two Arrhenius laws were constant. It was also observed for pure Ni oxidation for the transition between oxide scale growth kinetics controlled by grain boundary diffusion at low temperature and volume diffusion at higher temperature [27] or for the transition between transition alumina and alpha alumina on NiAl [24][28].

To explore the kinetic transient regime between the two laws described just before, a second SMT-TGA with fewer dwells and lower mass gains was performed at 900-1050-900°C. The first two dwells were shorter than in the first SMT-TGA experiment and were also shorter than the third dwell of this new multiple temperature TGA. Of particular interest are the k_p constant determined from the analysis of the mass gain curve of this three dwells SMT-TGA. The k_p values determined on the two dwells at 900°C (the first short and the second long after the dwell step at 1050°C) appear to be strongly different. The k_p value for the second dwell at 900°C is more than one order of magnitude lower than the one determined for the first dwell at 900°C. This value is also quite lower than the one evaluated from the first SMT-TGA. This difference clearly shows that a kinetic transient regime takes place during the oxidation of the AM1 alloy. The decrease of the k_p constant with time during the 950 and 1050°C dwells of the first SMT-TGA results also of the transitory stage. Isothermal thermogravimetric analyzes were carried out to understand the deviations in the values of k_p obtained by SMT-TGA, and to study the nature of the transient regime evidenced by the SMT-TGA.

Isothermal oxidation

Isothermal thermogravimetric analyses were realized to first confirm the k_p values obtained with the SMT-TGA. Mass gains have been corrected to remove the buoyancy effect. The apparent mass gain due to the buoyancy effect can be quantified on each sample by differentiating between the mass gain at the end of the isothermal dwell and the mass gain after the cooling [29]. The assumption is made that the mass gain due to oxidation during cooling is negligible compared to the mass gain during heating and during the high temperature dwell. Thus, the recording of the cooling phase at the end of isothermal TGA makes it possible to correct the mass gain curve for the buoyancy effect by simply subtracting the mass change during cooling. The corrected signal thus makes it possible to estimate the mass gain during heating.

Fig. 4a presents the different isothermal thermogravimetric analyses realized at constant temperature between 800°C and 1200°C. The curves have been corrected to remove the buoyancy effect and the mass at t=0 corresponds to the actual mass gain during heating. Fig. 4 b presents a zoom of the first ten hours. As the heating rate is always 60°/min, increasing the isothermal temperature dwell of course increases the mass gain during heating. The shape of the curve over the temperature range 950 to 1100°C clearly shows the presence of a fast transient regime before the establishment of the parabolic regime. The curve obtained at 1050°C gives a good illustration of this observation. The oxidation rate appears very fast during the first hour, then a slower rate is observed leading to a mass gain during the first hour which is roughly the same than as the mass gain between 1 h and 140 h. For isothermal TGA in the 950-1100°C range, the presence of this first faster kinetic regime leads to the fact that the total mass gains after 100 h of oxidation are all in the same range. However, the final slopes of the different curves are really different. Therefore, the parabolic constants at the end of the dwells are also different.

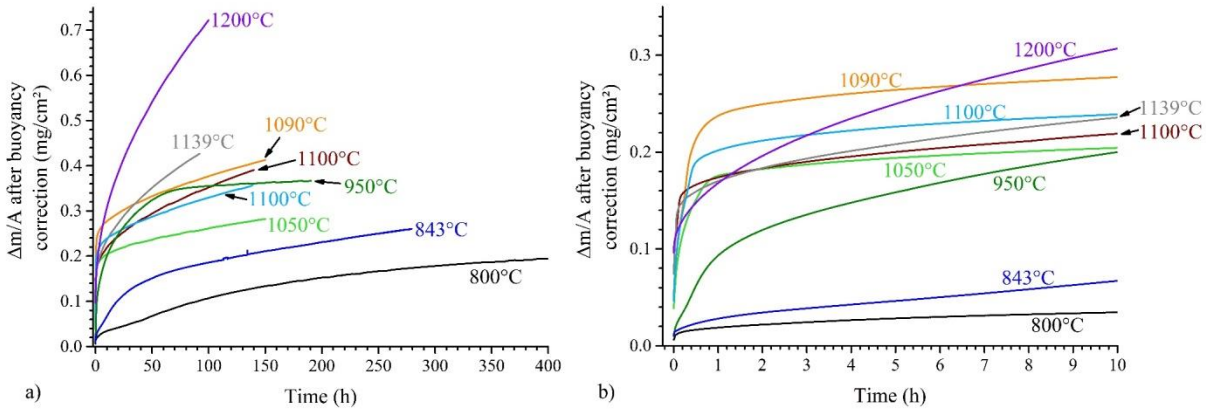

Fig. 4. a) Isothermal thermogravimetric analyses realized on AM1 in flowing synthetic air corrected to remove the buoyancy effect, b) zoom on the first ten hours. The mass gain at t=0 corresponds to the actual mass gain during the heating at 1°C/s to the dwell temperature.

The complete parabolic law was used at the end of isothermal oxidation to determine parabolic rate k_p. Results are plotted as orange dots in the Arrhenius plot in Fig. 2. At temperatures superior to 1000°C, the k_p values are in good agreement with k_p values estimated with SMT-TGA. This validates the SMT-TGA method as a fast means to determine k_p values in this highest temperature range. Compared to the literature data, the k_p values of AM1 alloy at temperatures above 950°C are a little bit lower than the one reported for the exclusive growth of α-Al_2O_3 scales on β-NiAl intermetallic [24,30]. This slightly lower k_p obtained for the AM1 could be attributed to the presence of hafnium in the AM1 alloy. Indeed, Hf can be found in grain boundaries of α-Al_2O_3 [6] and is known to have a beneficial effect on the oxidation kinetics of Ni-Al [31,32].

The k_p value determined at the end of the 950°C dwell by the isothermal TGA is one order of magnitude lower than the one determined with the SMT-TGA, Fig. 2. One can notice that the k_p value determined at the end of the 950°C long dwell follows the same Arrhenius law than the k_p values at higher temperatures. This shows that if the oxidation test is long enough and if the k_p constant is evaluated at the end of the mass gain curve, the rate limiting step for the oxide scale growth is the same than the one governing higher temperatures oxidation. The fact that for isothermal oxidation performed at 843 and 800°C, the k_p values are higher than the Arrhenius law determined for higher temperatures could be attributed to the fact that respectively 200 and 400h durations may be too short at these temperatures to be out of the kinetic transient regime. Hence, at these lower temperatures (below 950°C), the transient regime appears to last much longer than at higher temperature.

Characterization of oxide scales

Five samples from the isothermal TGA experiments were chosen to be characterized by XRD and to be observed in cross-section by SEM and EBSD. The time and temperature of oxidation of these samples were chosen to reflect the diversity of oxide scales formed on AM1 alloys in the temperature range tested. Fig. 5 shows the XRD diagrams of the samples oxidized at 1100°C for 10 min (a) and 140 h (b), at 950°C for 20 h (c) and 190 h (d) and at 800°C during 400 h (d).

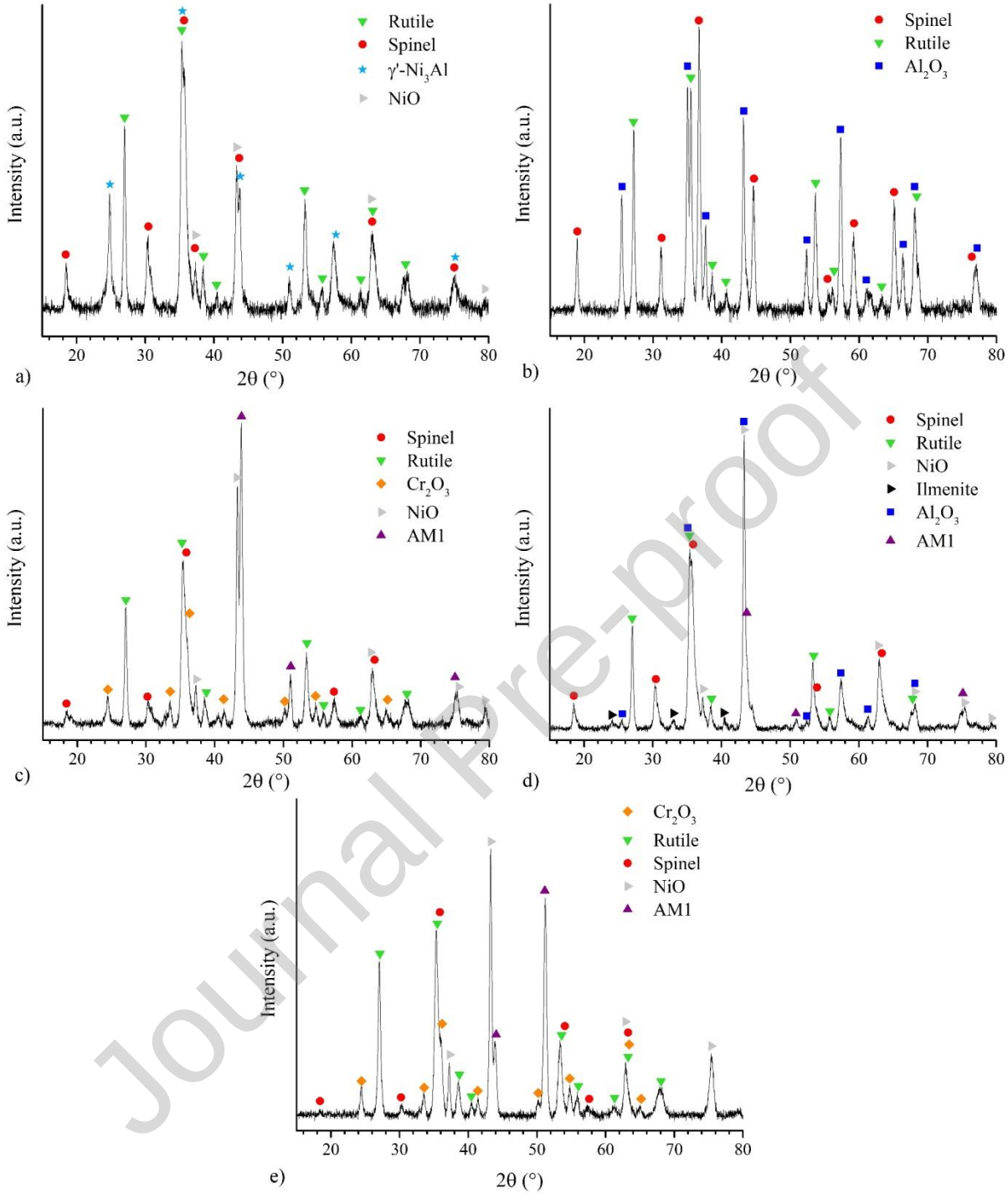

Fig. 5. XRD patterns of oxidized AM1 samples, a) 10 min at 1100°C, b) 140 h at 1100°C, c) 20 h at 950°C, d) 190 h at 950°C and e) 400 h at 800°C.

Rutile ($(Cr,Ti,Ta)O_2$) and spinel ($Ni(Al,Cr)_2O_4$) oxides are present on all the samples, regardless of oxidation time or temperature. The same oxides, i.e. spinel, rutile, chromia (Cr_2O_3) and bunsenite (NiO) are present on samples oxidized 20 h at 950°C and 400 h at 800°C. After 140 h at 1100°C, the oxide scale is composed of rutile, spinel and α-alumina. At 950°C, the XRD analysis shows that spinel, rutile, α-alumina (Al_2O_3), bunsenite and ilmenite ($NiTiO_3$) are found on AM1 alloy after an oxidation time of 190 h. With these five XRD analyses, α-alumina is only detected at 1100 and 950°C after 140 and 190 h of oxidation, respectively.

At 800 and 950°C, no visible change can be noticed in the spinel lattice parameter, which corresponds to the spinel $NiCr_2O_4$. At 1100°C, the lattice parameter of the spinel decreases with the oxidation time. It drops from 8.32 Å after 10 min of oxidation to 8.12 Å after 140 h of oxidation. In the literature, the lattice parameter of $NiCr_2O_4$ and $NiAl_2O_4$ are respectively reported to be 8.3155 Å [33] and 8.0475 Å [34]. Hence, the composition of the spinel in the scale formed on the AM1 alloy after a short period of oxidation at 1100°C seems to be $NiCr_2O_4$ while after 140 h the lattice parameter of the spinel seems to be closer to $NiAl_2O_4$. This phenomenon may be attributed to a chromium depletion in the oxide layer with time. It could be linked to the oxidation of chromia into a volatile oxide. Volatilization of Cr oxide is a possibility, but it was not possible to evaluate it quantitatively from the TGA curves.

Cross-section characterizations were realized in order to observe the nature and morphology of the oxide scales. The oxide scale is too thin (1-2 µm thickness) to precisely identify the oxide sublayers by EDX. Then, an EBSD analysis (Fig. 6a) was conducted on the cross-sections of the sample oxidized 140 h at 1100°C to clearly identify the position and the nature of the oxide phases identified by XRD.

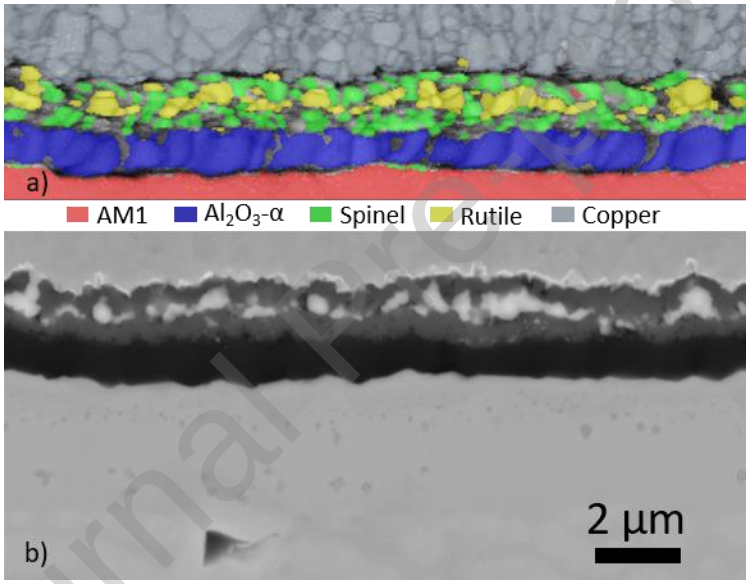

Fig. 6. Cross-section of the oxide layer formed on AM1 after 140h of oxidation at 1100°C, a) EBSD mapping, b) SEM-BSE micrograph.

Fig. 6 shows that the oxide scale is composed of α-alumina at the metal/oxide interface, surmounted by a spinel layer, and rutile precipitates are present in the spinel layer. EDS analyses (not shown) show that the rutile phase is rich in Cr, Ta and Ti. Rutile precipitates appear much brighter than the metal on SEM BSE micrographs due to the presence of tantalum in these precipitates. It can be noted that the α-alumina layer is composed of a single grain of alumina in thickness and grains larger in width than for the spinel layer. Beneath the oxide scale, a zone depleted in γ' is present. Some precipitates are observed beneath the oxide layer. EDS analyses (not shown) show that these precipitates are rich in titanium. This type of precipitate is likely titanium nitrides which would have formed by internal nitridation during the first hours before the oxide layer is sufficiently protective to prevent the diffusion of nitrogen inwards, as already shown for the oxidation of Ni-base single crystal alloy [35].

Fig. 7 shows SEM-BSE micrographs of cross-sections of characterized samples. Alumina is visible on the cross-sectional micrographs of the five samples analyzed, although α-alumina is not visible by X-ray diffraction for the oxidized samples 400 h at 800°C and 20 h at 950°C.

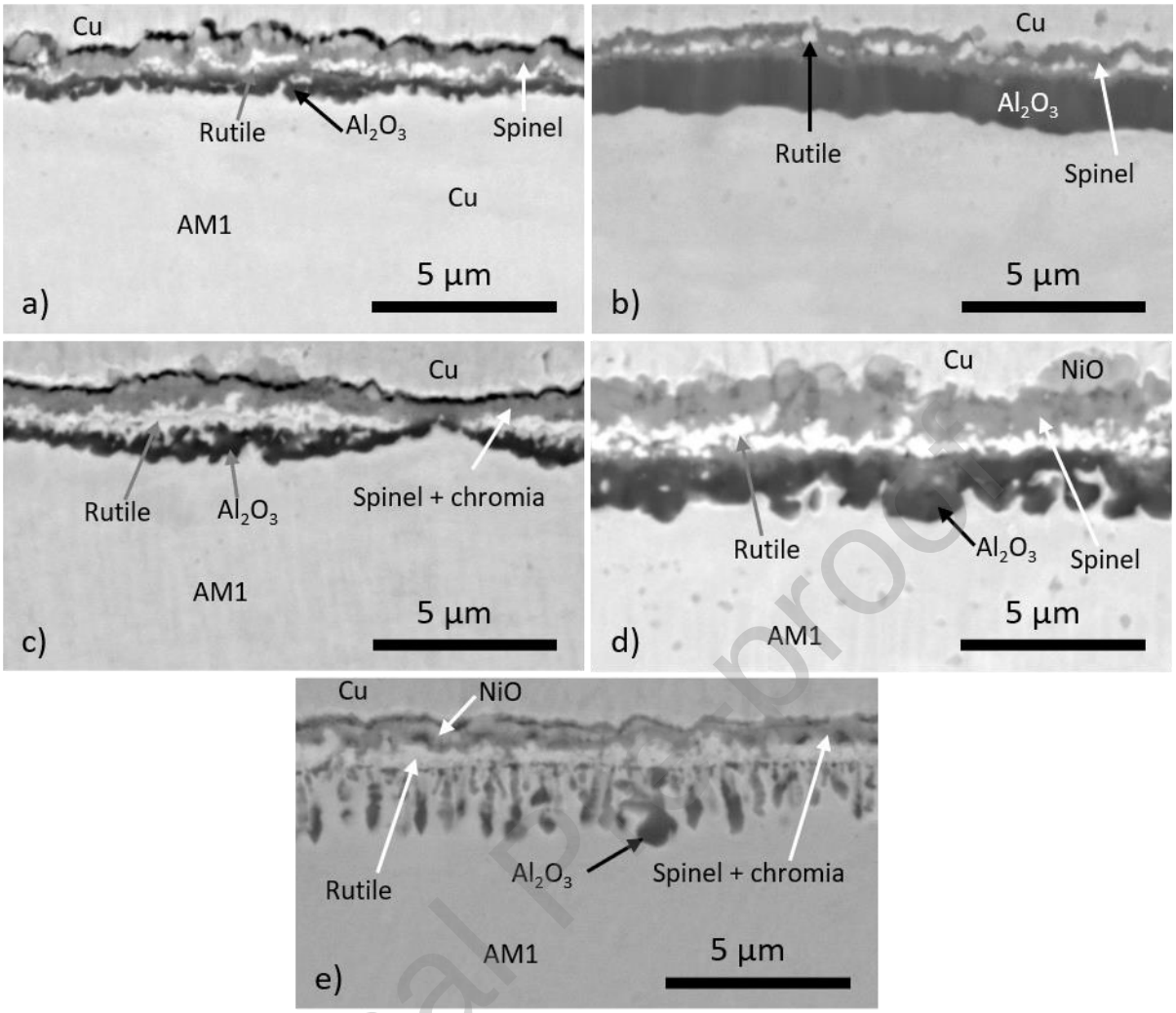

Fig. 7. SEM-BSE micrographs of the cross-sections of the oxide layers formed on AM1 alloy after, a) 10 min at 1100°C, b) 140 h at 1100°C, c) 20 h at 950°C, d) 190 h at 950°C and e) 400 h at 800°C.

Depending on the temperature and the oxidation time, the morphology of the alumina layer is different. At 800°C (Fig. 7e), alumina forms elongated precipitates in the alloy beneath and perpendicular to the metal/oxide interface and is generally connected to this interface. Hence, under these conditions, the alumina layer is not continuous. At 950°C (Fig. 7c and 7d) whether after 20 h or after 190 h, the alumina layer appears continuous and convoluted. At 1100°C after 10 min the alumina layer is convoluted (Fig. 7a) while after 140 h, the layer is thicker and flatter (Fig. 7b).

Image analyses were performed to evaluate the thickness of the different oxide sublayers on the samples oxidized at 950 and 1100°C, results are presented in Table 3. For the sample oxidized at 800°C, the fineness of the oxides and the low contrast between rutile and metal make it difficult to perform reliable image analysis.

At 1100°C, the main difference between the oxide layers obtained after 10 min and 140 h of oxidation is the increase in the thickness of alumina. While at 950°C, the thickness of spinel, alumina and NiO increases between 20 and 190 h of oxidation.

To synthesize the oxide scales characterizations, the oxide scale formed on the AM1 alloy at high temperature (above 1050°C) is mainly formed of α-alumina, spinel and rutile while at

lower temperature (below 1050°C) the oxide layer is mainly formed of chromia, spinel, rutile, bunsenite, α-alumina and ilmenite (at 950°C). After 400 h at 800°C, alumina precipitates are formed but there is no continuous layer of alumina. This effect of the temperature on the morphology of alumina has already been reported in the literature [36].

Model

The study of the oxidation kinetics of the AM1 alloy has shown a transition from a first fast oxidation regime with short times to a slower oxidation regime when the oxidation time increases. The first fast transient regime is much shorter when the temperature increases. Observation of the oxide layers formed under different conditions revealed a change in the morphology of the alumina layer with time and temperature that can explain the transition between the two regimes. A model is then proposed in the following part to take into account these two observations. The objective of the modeling is to predict the oxidation kinetics of the AM1 alloy for all temperatures and durations, with a single set of kinetic parameters.

To simplify, the model only considers two types of oxides growing on the alloy, i.e. α-alumina and a transient oxide. It is assumed that the rapid oxidation regime is due to the growth of a covering layer made of transient oxide at the surface of the alloy. Under this layer, precipitates of α-alumina are growing in thickness but also laterally. At the location of these precipitates, the growth of the oxide layer is controlled by the diffusion of elements through the α-alumina precipitates, which implies that the growth of the transition oxides above the precipitates considerably slows down. In order to simplify the model, the transition oxide layer above an alumina precipitate is considered to no longer grow. The surface occupied by these internal alumina precipitates increases with time until the surface is completely covered, forming a continuous protective layer of alumina. When a continuous α-alumina layer is formed, the transition oxide layer no longer grows and the growth kinetics of the oxide layer is the same as for an α-alumina layer. With such mechanisms, the model makes use of some simplifying assumptions: the growth of transition oxide and α-alumina is parabolic; the α-alumina precipitates nucleate at the beginning of heating, they are randomly distributed on the surface and there is no nucleation of new precipitate over time. The radius of the precipitates increases linearly with time during the high temperature dwell. The initial surface coverage, at the beginning of the high temperature dwell, is estimated from the mass gain during heating. The growth of transient oxide is stopped when they are above an α-alumina precipitate.

With such assumptions, the mass gain per unit surface area at the time i, of transient oxide $\Delta m1_i$ on top of a surface without alumina precipitate can be defined with Eq2.

$$\Delta m1_i = \sqrt{m_0^2 + k_{p1} \times t_i} \qquad \text{Eq2}$$

With t_i the time from beginning of the dwell, m_0 the mass gain during the heating process and k_{p1} the parabolic constant corresponding to the thickening of the transient oxide.

The mass gain per unit surface area at the location of alumina precipitates $\Delta m2_i$ is defined with Eq3.

$$\Delta m2_i = \sqrt{k_{p2} \times t_i} \qquad \text{Eq3}$$

with k_{p2} the parabolic constant corresponding to the thickening of α-Al_2O_3.

Evans [37] proposed a method to represent the kinetics of covering of a surface by precipitates spreading out as expanding circles. This model assumed the presence of nuclei randomly distributed on the initial surface and a linear growth of the radius nuclei. The

surface ratio θ represents the surface covered with precipitates, its evolution with time can be described with Eq4.

$$\theta_i = 1 - e^{-k_t \times (t_i + t_0)^2} \text{ with } t_0 = \frac{m_0^2}{k_{p1}} \qquad \text{Eq4}$$

with k_t a parameter of the model characterizing the kinetics of spreading of alpha-alumina, t_0 the time needed to form the same mass gain during the high temperature dwell than the mass gain m_0 during heating. t_0 allows to take into account the advancement of the transition during the heating process, which one is especially important at high temperatures. Indeed, the mass gain during heating cannot be neglected. In addition, as the transition is faster at higher temperature, neglecting the heating would lead to an error in the rate of the transition between the two regimes at the highest oxidation temperatures.

The model assumes that the fraction of surface, θ, is covered with an oxide scale which grows according to the parabolic law of α-alumina and that the rest of the surface, 1-θ, has an oxide scale which grows according to the parabolic law of transition oxides. The mass gain over time is then calculated by incrementing the time from the beginning of the isothermal stage with the following equation (Eq5).

$$\Delta m_i = \Delta m_{i-1} + (\Delta m1_i - \Delta m1_{i-1}) \times e^{-k_t \times (t_i + t_0)^2} + (\Delta m2_i - \Delta m2_{i-1}) \times \left(1 - e^{-k_t \times (t_i + t_0)^2}\right) \text{ Eq5}$$

with i the time increments an Δm_i the total mass gain per area at the time step i. To summarize, the input parameters of the model are only 4 : m_0, k_{p1}, k_{p2}, and k_t. The model is fitted on each isothermal thermogravimetric data in order to obtain the values of the 4 parameters able to describe the oxidation kinetics for all the tested temperatures. Fig. 8 shows an example of fitting gravimetric results obtained for the 40 first hours at 1000°C with the oxidation model. It gives the evolution with time of total mass gain, as well as the part of the mass gain due to the formation of transient oxide and the one due to alumina. The evolution with time of the ratio of the surface covered with alumina, θ, is also given. Schematic images of the cross-sections of the oxide layer as a function of time are also given as guidelines.

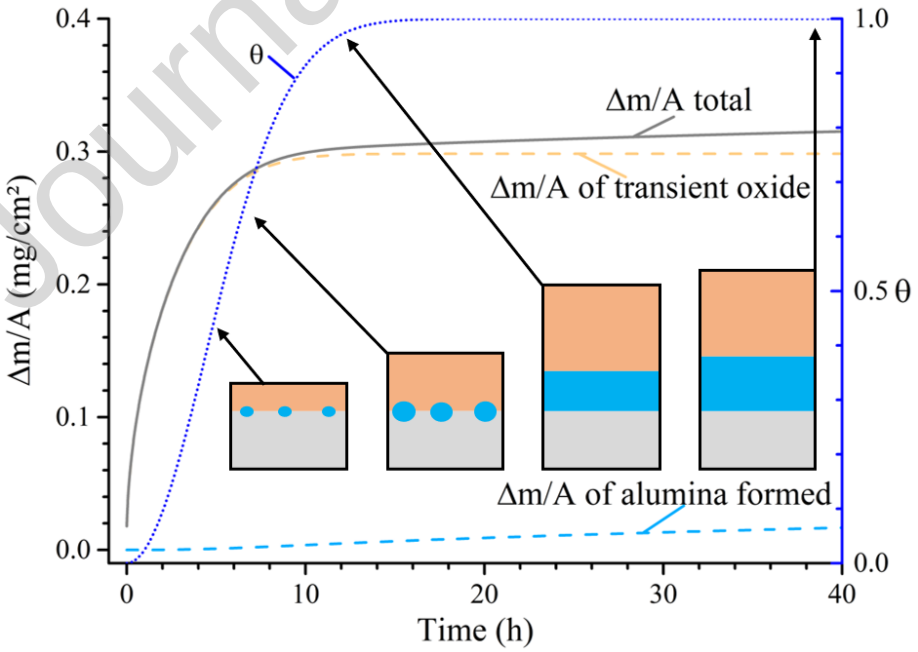

Fig. 8. The evolution of mass gain per area as a function of time simulated with the model for the first 40h of the 1000°C oxidation. The mass gain corresponding to the growth of transition oxides and to the growth of α-alumina is plotted. The variation of alumina coverage θ as a

function of time is represented with schematic images of the cross-sections of the oxide layer as a function of time as guidelines.

Because the growth of the oxides is supposed to be controlled by diffusion, Fig. 9a, 9b and 9c show the evolution of the parameters in an Arrhenius plot. From these values, it is remarkable that three Arrhenius laws can be fitted for each input kinetic parameter of the model. The following laws are obtained:

$$k_{p1} = 1.1 \times 10^{7} \times e^{\frac{-3.6\times10^{5}}{R\times T}} \text{ mg}^2\text{.cm}^{-4}\text{.s}^{-1} \qquad \text{Eq6}$$

$$k_{p2} = 7.1 \times 10^{8} \times e^{\frac{-4.2\times10^{5}}{R\times T}} \text{ mg}^2\text{.cm}^{-4}\text{.s}^{-1} \qquad \text{Eq7}$$

$$k_{t} = 4.5 \times 10^{27} \times e^{\frac{-8.9\times10^{5}}{R\times T}} \text{ s}^{-2} \qquad \text{Eq8}$$

Fig. 9 also compares the evolution with temperature of the various kinetic parameters and the evolution of the adjusted laws (Eq 6-7-8). The evolution of the adjusted parabolic rate constants, k_{p1} (Fig. 9a) and k_{p2} (Fig. 9b), are in fairly good agreement with the k_p values from the literature for α-alumina [24,30] and chromia [25]. The Fig. 9c compares the values (points) of the transition kinetics parameter k_t, adjusted from the nine different isothermal experiments and the Arrhenius law proposed for this parameter in the model (Eq8).

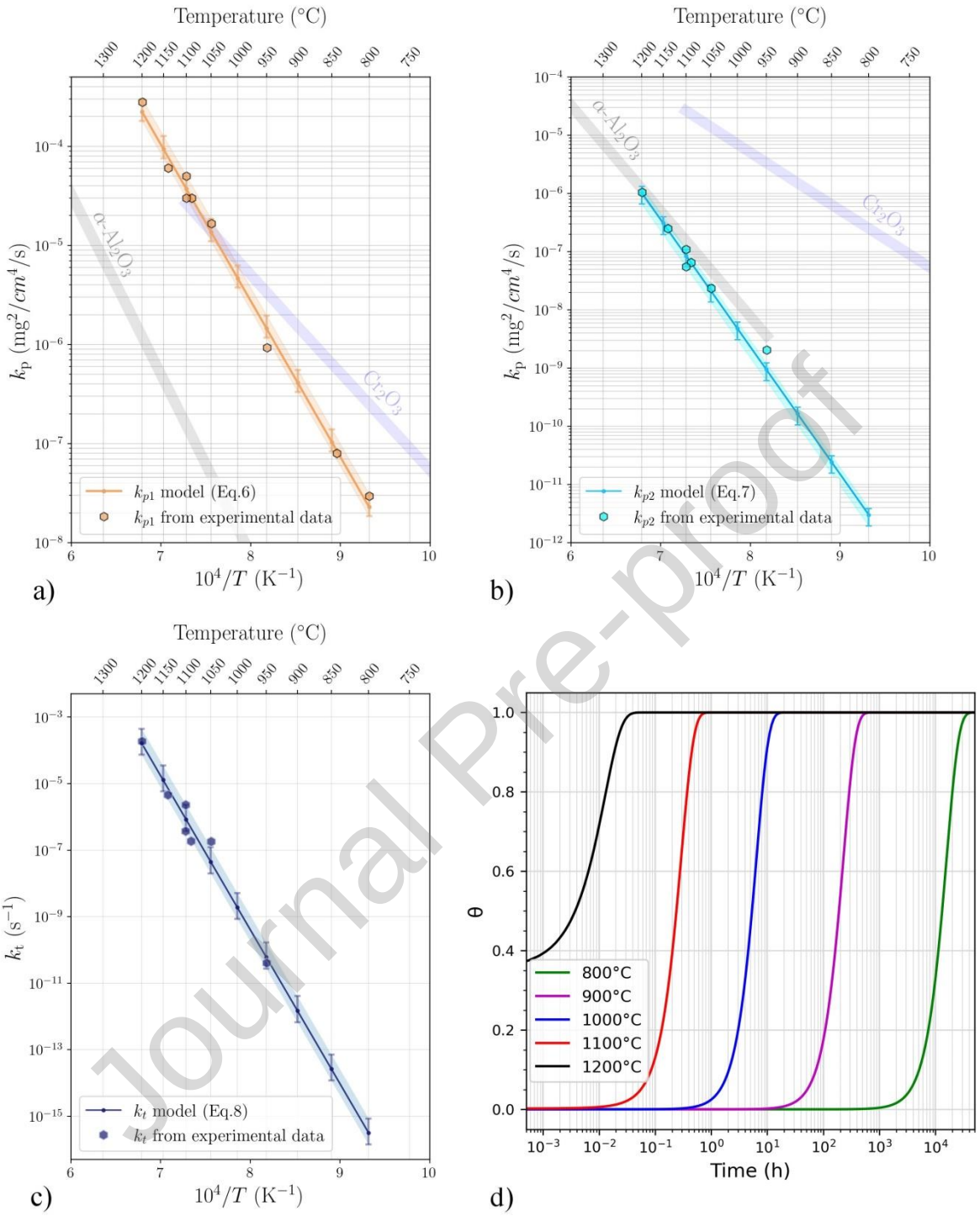

Fig. 9. Arrhenius plots of three laws chosen for three key parameters of the model (a), k_{p1}, (b) k_{p2} and (c) k_t. (d) Evolution of the surface ratio covered with alumina precipitates θ (calculated with the model) as a function of time for different temperatures.

Two isothermal tests were carried out at 1100°C. The adjustment of these data with the model makes it possible to test the reproducibility of the values of k_{p1}, k_{p2} and k_t for a given temperature. The percentage difference between these fitted parameters and the value obtained by the model at 1100°C gives us an estimate of the uncertainty of the model at 1100°C. The assumption of constant uncertainty over the temperature range studied was made, by considering that the Arrhenius laws corresponding to the maxima and minima of the

values of a parameter had the same activation energy. These percentages of uncertainty are presented in Table 4. This makes it possible to define a confidence interval for the model. For this, the upper limit of the model is obtained with the maximum values of k_{p1} and k_{p2} and the minimum values of k_t, the reverse is done for the lower limit of the model.

A larger uncertainty of the adjusted k_t than for k_p is observed. For this latter parameter, following the Evans equation [37], it can be defined with the following equation Eq9.

$$k_t = \pi\omega\nu^2 \qquad \text{Eq9}$$

where ω is the surface density of nuclei, and ν is the radial rate of growth of nuclei. k_t gathers both the density of nuclei and their radial growth rate. These two parameters can be impacted by the surface preparation and by local variation of composition which can lead to deviation of k_t. That could explain local deviations of the k_t points from the Arrhenius law. But, as shown by Fig. 9c, the global evolution of k_t points follows an Arrhenius law all over the temperature range studied.

The three parameters of the model globally follow Arrhenius laws very well, as shown in Fig. 9. Furthermore, the k_{p1} parameter is close to the k_p values of the formation of chromia and close to the k_p values obtained experimentally at low temperatures (<900°C) with our isothermal TGA. In addition, the k_{p2} parameter is close to the k_p of α-alumina and is also very close to the k_p values determined experimentally for high temperatures (>900°C). These trends show that the proposed model is in good accordance with all the kinetics measurements over the wide temperature range studied, from 800°C to 1200°C.

Fig. 9d shows the evolution with time of the ratio of the surface θ covered with α-alumina for different temperatures, calculated with the Arrhenius law obtained for the k_t parameter. It illustrates that the time needed to reach the end of the kinetic transient regime, i.e, when the θ ratio reaches 1, evolves strongly with temperature. The duration is barely reachable at lab scale for 800°C. At intermediate temperatures 900°C-950°C, the AM1 alloy will be considered as an alumina-forming alloy (complete covering of the surface by alumina, θ=1) depending on the oxidation duration. At 1000°C, about 10h oxidation is needed for the alumina layer to be formed on bare AM1 alloy. At higher temperatures, at 1100°C and over, this time drops under 1 h of oxidation. At the highest temperatures, e.g. at 1200°C here, the transition is too fast to be observed when holding at high temperature, and has already occurred largely on heating.

With the values of k_{p1}, k_{p2} and k_t and their evolutions with the temperature, oxidation during non-isothermal conditions can be estimated. The model could then be used to simulate a complete TGA experiment by incrementing the time from the beginning of the heating process. In this case, the temperature varies with time and the θ value evaluation must consider this change (Eq10). In the present case, m_0 was determined with a temperature rise rate of 1°C/s.

$$\theta_i = 1 - e^{-k_t \times \left(t_{i-1} - t_i + \sqrt{\frac{ln(1-\theta_{i-1})}{-k_t}} \right)^2} \qquad \text{Eq10}$$

In order to verify the validity of the model, the parameters of k_{p1}, k_{p2}, k_t obtained with Arrhenius laws are used to plot the evolution of the mass gain as a function of time at different temperatures in order to compare them with the results of the isothermal TGA performed. This is done taking into account the heating part of the TGA experiments. The

comparison of isothermal TGA and model-simulated mass gains at 800, 950, 1050, and 1200°C is shown in Fig. 10.

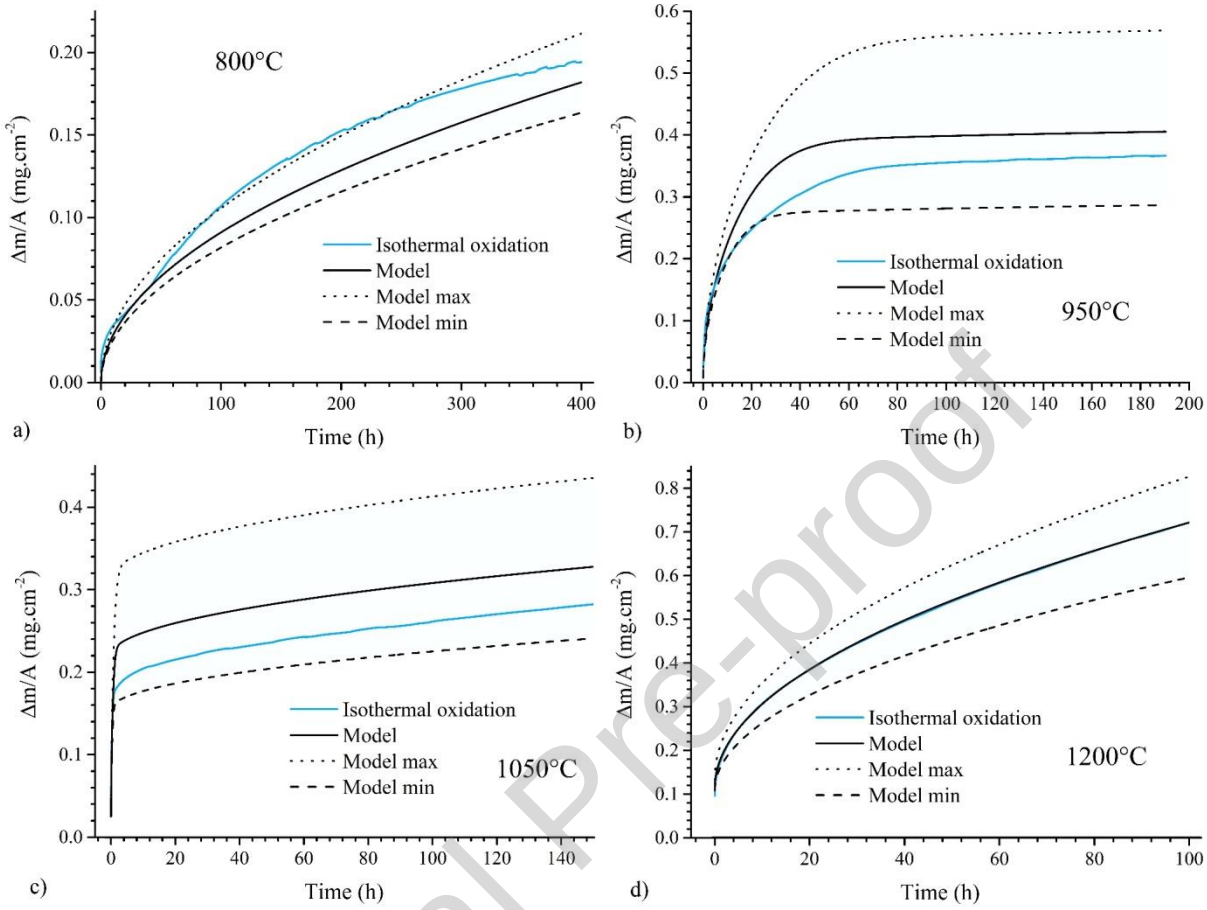

Fig. 10. Comparison between the oxidation simulations proposed by the model and the mass measurements during the isothermal TGA tests carried out, a) at 800°C, b) at 950°C, c) at 1050°C and d) at 1200°C (model and data are superimposed).

The experimental curves are in good agreement with the model results. At 1050°C, the mass gain curve calculated by the model is above the experimental values. This difference is due to the variability of the k_t parameter. Indeed, a slight overestimation of the transition time leads to an increase of the mass of transient oxide gained during the transient regime.

Discussion

Fig. 11 compares the evolution of the parabolic constant k_p estimated from experimental isothermal TGA experiments and the ones estimated from TGA curves simulated with the model. In both cases, the values of k_p are determined with the complete parabolic law [19] (Eq1). They are estimated at different times of the curve (10 min, 30 min, 1 h, 10 h, 50 h, 100 h, 200 h, 400 h). Results obtained are plotted as crosses (X) for k_p values obtained from analysis of the experimental TGA curves and as lines for k_p values obtained from analysis of simulated TGA curves calculated with the model. A good agreement can be observed between the experimental k_p (X) and the k_p determined on the curves calculated with the model (lines).

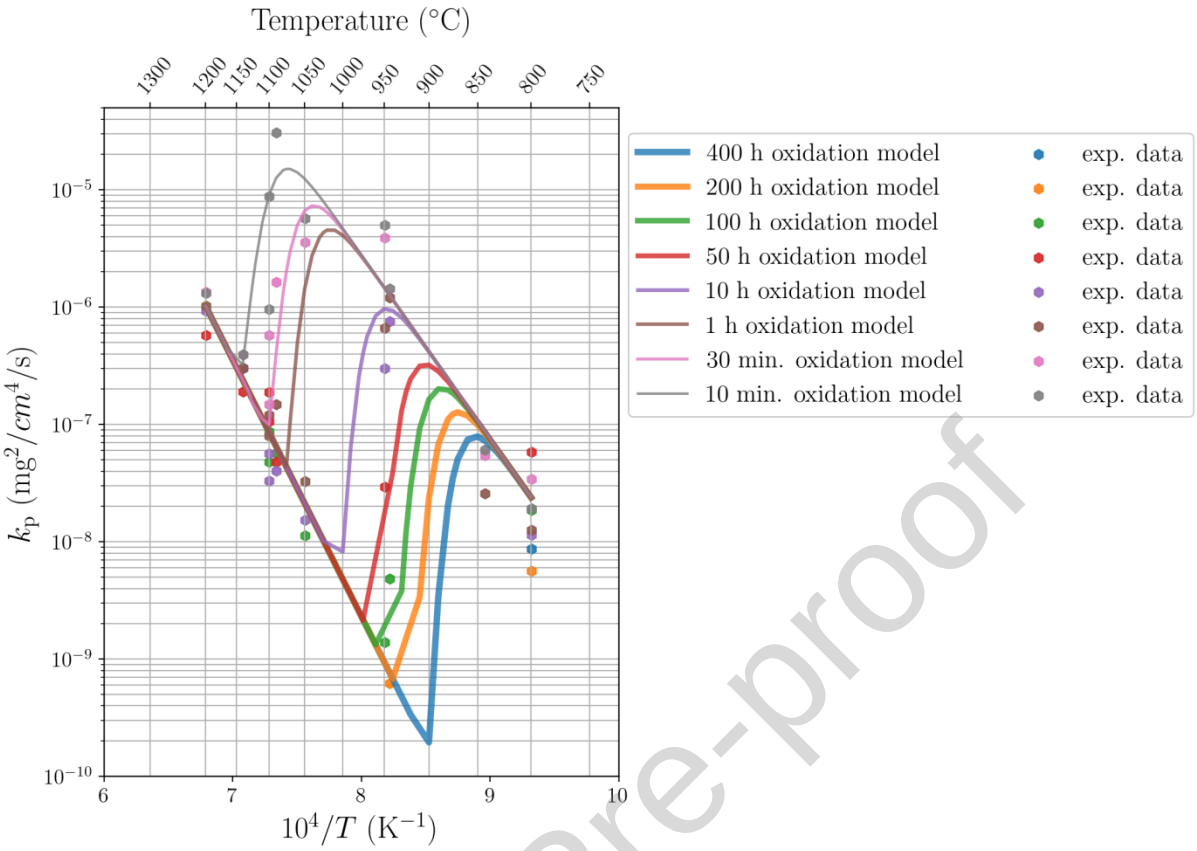

Fig. 11. Arrhenius plot of the parabolic rate constant k_p determined from the analysis of the isothermal TGA experiments at different times (dots) and calculated using the model (lines) for different oxidation times.

The k_p values are plotted in an Arrhenius diagram. This representation allows to visualize the evolution of the k_p as a function of the temperature and the oxidation time depending on the importance of the kinetic transient regime on the k_p estimation. It shows that over the intermediate range of temperature, the comparison of different studies will be difficult because the estimation of the k_p constant will be strongly affected by the oxidation duration. For example, at 950°C, oxidation of 10h will lead to a k_p estimation of about 10^{-6} mg^2.cm^{-4}.s^{-1} whereas, with 100h oxidation the k_p will be estimated to be more than two orders of magnitude less. The shorter will be the experiment, the larger will be the temperature range inside which the estimation of k_p will suffer from this kind of discrepancies.

Since Fig. 11 shows the values of k_p at different oxidation times as a function of temperature, it is possible to find the Arrhenius laws of the two parameters k_{p1} and k_{p2}. But more importantly, this representation allows us to see the evolution of the constant k_p determined for a fixed time between the two oxidation regimes. During the isothermal oxidation of AM1, the constant k_p varies from the Arrhenius law of transition oxides (k_{p1}) to the Arrhenius law of α-alumina (k_{p2}) as a function of the oxidation time and varies more rapidly as the temperature increases.

For Ni-base single crystal superalloys, the use of a time-temperature-θ diagram is more suitable and can be plotted with the data generated by the model. This type of representation has already been used to delineate the transition alumina formation domains [38] and is given for the present model for the AM1 alloy in Fig. 12. In the same figure are depicted the different isothermal TGA experiments which have been done and the nature of the oxide

scales determined by XRD analysis for the corresponding samples as well as cross sections SEM observation for three chosen points. This allows to correlate the oxidation kinetics and the oxide scale microstructure.

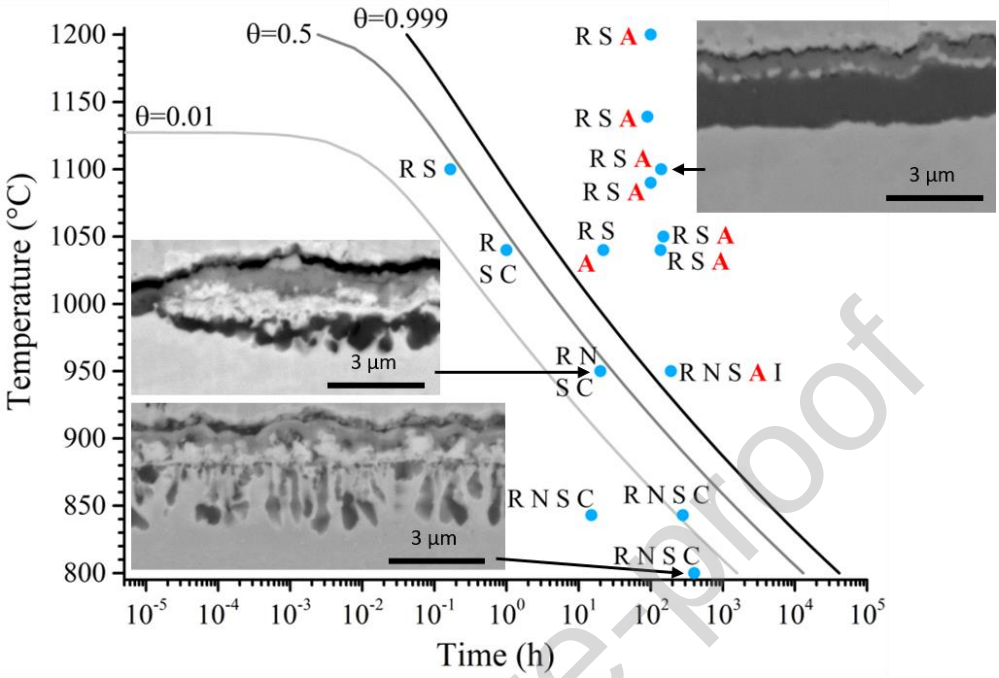

Fig. 12. Time-temperature-θ diagram. Dots represent isothermal oxidation and letters represent the oxide identified by XRD after oxidation (R = rutile, S = spinel, A = Al_2O_3, C = Cr_2O_3, N = NiO, I = ilmenite). Lines represent the different values of θ calculated with the model.

This diagram can be used to estimate the oxidation time required to switch from the transient to the stationary regime. The beginning of the transition was estimated at a θ value of 0.01 corresponding to 1% of the surface controlled by diffusion in alumina. In our case, we considered that the transition was finished when the percentage of surface controlled by diffusion in α-alumina was 99.9% (θ = 0.999). It corresponds to the moment when the mass of oxygen fixed on the sample by the transition oxides represents approximately 10% of that fixed by the growth of α-alumina.

It can be noticed that X-ray diffraction allows to detect α-alumina only after the end of the transition, whereas α-alumina can be clearly observed on SEM cross-sections during the transient regime.

At low temperature, the transient regime is very long, for example at 800°C, the oxidation time would be more than 30 kh (i.e. 3.4 yrs) to reach the stationary regime. Because of this long duration, no experimental data is available to confirm this. At low temperatures, the time required to complete the transition can be of the same order of magnitude as the life of a part in service, in this case, the transient regime clearly must be taken into account when designing these parts.

Regarding the validity of the model, several hypotheses can be discussed. EBSD results show that the α-alumina layer is composed of a single grain in thickness, all of the same size, which seems to confirm the absence of nucleation of other α-alumina grains than those present at the beginning of the transition. The presence of α-alumina precipitates from the beginning of the dwell is difficult to verify but at low temperature, the presence of α-alumina from the beginning is unlikely. In this study, transition alumina oxide was never observed but it could

be present at short time and low temperature [10]. Looking at the cross-section SEM images of the samples oxidized for a short time, (i.e. shorter than the time needed to complete the transition) (see Fig. 7c) and e)), the interface seems to be covered with more alumina than what is expected from the model prediction. In this case, when alumina is formed by internal oxidation, its growth kinetics is controlled by oxygen diffusion through the metal layer which can be seen between the transient oxide and alumina. Then, at this stage, the growth of alumina is not controlled by the diffusion of elements through alumina itself, and the growth of the transition oxide layer is neither controlled by the diffusion of cations through an alumina layer. This fact does not call into question the model because in this case this internally growing alumina is considered as a transition oxide. In this case, the assumption of linear growth of α-alumina precipitates can be supported by the observations of Barth et al. [39]. During the oxidation of β-NiAl in the presence of titanium and/or silicon and/or yttrium, the radial growth of alumina precipitates follows a linear law in time [39].

Conclusions

The purpose of this study was to investigate the oxidation behavior of the bare AM1 Ni-base single crystal superalloy over a large temperature range. A stepwise multi-temperature thermogravimetric analysis (SMT-TGA) was used to obtain the oxidation behavior of the alloy over the temperature range 750 to 1300°C. This method, which consists in chaining the temperature steps, is faster than performing multiple isothermal oxidation experiments, and requires only one sample to obtain the parabolic oxidation constants of AM1 at several temperatures. In this study, isothermal thermogravimetric analyses were performed to assess the results obtained with SMT-TGA. The parabolic rate constants k_p obtained with the two types of tests are close to each other, which validates the use of SMT-TGA analysis. A transitory regime in the oxidation kinetics is evidenced by both isothermal and SMT-TGA. The duration of this transient regime decreases with increasing temperature. This kinetic transient regime was correlated to the microstructural observations. XRD and cross-section characterizations allowed to highlight an evolution of the morphology of the oxide layer as a function of time and temperature. At long time and high temperatures (140 h at 1100°C), a continuous and protective alpha alumina layer is formed. At lower temperatures and shorter times (10 min at 1100°C, 20 and 190 h at 950°C), the alumina layer is convoluted and seems continuous. At low temperatures, and even for relatively long times (400h at 800°C), alumina is present as internal precipitates and does not form a continuous protective layer. A Comparison of multiple isothermal oxidation tests with the SMT-TGA test shows that SMT-TGA allows drawing the complete picture of the kinetic oxidation behavior of the AM1 alloy in a single experiment.

A model that takes into account the kinetics of the transition from transient oxides growth to protective alumina was built. This was done in order to be able to simulate the oxidation of AM1 over the whole temperature range 800-1200°C. This model assumes that the morphological evolution of the alumina layer observed causes the transition in oxidation rates. Only 4 parameters are necessary, and they can be fitted on experimental data. 3 of the parameters characterize the growth kinetics of the transient oxide, the growth kinetics of the protective oxide and the transition rate between the two types of kinetic control. These 3 kinetics parameters follow Arrhenius laws. The physical meaning of these parameters can be validated because they can be relied on to the observation of the oxide scale microstructure.

The oxidation kinetic model proposed for AM1 shows a good agreement with experimental isothermal mass gain curves. Thanks to this model, it becomes possible to estimate the oxidation time necessary for a sample of AM1 to leave the transient regime. Results show that

over the lower temperature range explored 800°C-1000°C, whether the alloy is an alumina-forming alloy or not is dependent on the duration of oxidation and not only on the temperature. The model shows that very long isothermal experiments (up to tens and hundreds of thousand hours) would be necessary to check if the stationary regime can be reached at temperatures below 850°C.

This model may be applied to other superalloys than AM1 where the same phenomena are involved, i.e. a transition with time between the formation of transient oxide(s) (Ni-rich spinels, chromia, transient aluminas...) and the formation of a protective alpha alumina layer. Of course, the parameters k_{p1}, k_{p2} and k_t may have different values for different alloys. To obtain the parameters k_{p1}, k_{p2} and k_t for other alloys, it is necessary to fit the model on isothermal tests at different temperatures. The k_{p2} parameters which represent the oxidation rate of α-alumina could be close to those of AM1. But the k_{p1} and k_t parameters which respectively represent the oxidation rate of the transient oxide and the kinetics of coverage of the alpha alumina layer could be far to those of AM1. Performing at first a SMT-TGA experiment will indicate if there is an important role of the transient regime for a given superalloy. It will also give some first estimates of the model parameters.

Acknowledgements

This study was performed thanks to the financial support of Safran-Tech. The AM1 alloy was provided by Safran Aircraft Engine. The authors would like to thank Arnaud Proietti from the Raimond Castaing Microanalysis Centre for the EBSD analyses.

Data availability

The raw/processed data required to reproduce these findings cannot be shared at this time as the data also forms part of an ongoing study.

References:

[1] R.C. Reed, The Superalloys: Fundamentals and Applications, Cambridge University Press, 2008.

[2] J.H. Davidson, A. Fredholm, T. Khan, J.-M. Théret, Alliage monocristallin à base de nickel, French Patent (1983).

[3] K. Bouhanek, O.A. Adesanya, F.H. Stott, P. Skeldon, D.G. Lees, G.C. Wood, High temperature oxidation of thermal barrier coating systems on RR3000 substrates: Pt Aluminide bond coats, 639 (2001) 369. https://doi.org/10.4028/www.scientific.net/MSF.369-372.615

[4] P. Audigié, A. Rouaix-Vande Put, A. Malié, D. Monceau, High-temperature cyclic oxidation behaviour of Pt-rich γ-γ' coatings. Part I: Oxidation kinetics of coated AM1 systems after very long-term exposure at 1100 °C, Corrosion Science 144 (2018) 127-135. https://doi.org/10.1016/j.corsci.2018.08.050

[5] E. Fedorova, D. Monceau, D. Oquab, Quantification of growth kinetics and adherence of oxide scales formed on Ni-based superalloys at high temperature, Corrosion Science 52 (2010) 3932-3942. https://doi.org/10.1016/j.corsci.2010.08.013

[6] F. Pedraza, R. Troncy, A. Pasquet, J. Delautre, S. Hamadi. Critical Hafnium Content for Extended Lifetime of AM1 Single Crystal Superalloy. In: , et al. Superalloys 2020. The Minerals, Metals & Materials Series. Springer, Cham (2020) 781-788. https://doi.org/10.1007/978-3-030-51834-9_76

[7] B.A. Pint, K.L. More, I.G. Wright, P.F. Tortorelli, Characterization of thermally cycled alumina scales, Materials at High Temperatures 17 (2000) 165-171. https://doi.org/10.1179/mht.2000.024

[8] R. Orosz, U. Krupp, H.-J. Christ, D. Monceau, The Influence of Specimen Thickness on the High Temperature Corrosion Behavior of CMSX-4 during Thermal-Cycling Exposure, Oxidation of Metals 68 (2007) 165–176. https://doi.org/10.1007/s11085-007-9067-9
[9] M. Juez-Lorenzo, V. Kolarik, W. Stamm, H. Fietzek, Oxidation of nickel-based alloys in dry and water vapour containing air, Materials at High Temperatures 29 (2012) 229-234. https://doi.org/10.3184/096034012X13348393336892
[10] C.K. Sudbrack, D.L. Beckett, R.A. MacKay, Effect of Surface Preparation on the 815°C Oxidation of Single-Crystal Nickel-Based Superalloys, JOM 67 (2015) 2589-2598. https://doi.org/10.1007/s11837-015-1639-6
[11] M. Bensch, A. Sato, N. Warnken, E. Affeldt, R.C. Reed, U. Glatzel,. Modeling of the Influence of Oxidation on Thin-Walled Specimens of Single Crystal Superalloys. In Superalloys 2012 (eds E.S. Huron, R.C. Reed, M.C. Hardy, M.J. Mills, R.E. Montero, P.D. Portella and J. Telesman) (2012). https://doi.org/10.1002/9781118516430.ch36
[12] M. Bensch, A. Sato, N. Warnken, E. Affeldt, R.C. Reed, U. Glatzel, Modelling of High Temperature Oxidation of Alumina-Forming Single-Crystal Nickel-Base Superalloys, Acta Materialia 60 (2012) 5468-5480. https://doi.org/10.1016/j.actamat.2012.06.036
[13] K. Loeffel, L. Anand, Z.M. Gasem, On modeling the oxidation of high-temperature alloys, Acta Materialia 61 (2013) 399-424. https://doi.org/10.1016/j.actamat.2012.07.067
[14] S. Dryepondt, D. Monceau, F. Crabos, E. Andrieu, Static and dynamic aspects of coupling between creep behavior and oxidation on MC2 single crystal superalloy at 1150°C, Acta Materialia 53 (2005) 4199-4209. https://doi.org/10.1016/j.actamat.2005.05.018
[15] T.J. Nijdam, L.P.H. Jeurgens, W.G. Sloof, Modelling the thermal oxidation of ternary alloys—compositional changes in the alloy and the development of oxide phases, Acta Materialia 51 (2003) 5295–5307. https://doi.org/10.1016/S1359-6454(03)00381-1
[16] T. Gheno, D. Monceau, D.J. Young, Kinetics of breakaway oxidation of Fe-Cr and Fe-Cr-Ni alloys in dry and wet carbon dioxide, Corrosion Science 77 (2013) 246-256. https://doi.org/10.1016/j.corsci.2013.08.008
[17] H.V. Atkinson, Evolution of grain structure in nickel oxide scales, Oxidation of Metals 28 (1987) 353-389. https://doi.org/10.1007/BF00666728
[18] Z. Liu, W. Gao, A numerical model to predict the kinetics of anisothermal oxidation of metals, High Temp. Mater. Process. 17 (1998) 231-236. https://doi.org/10.1515/HTMP.1998.17.4.231
[19] D. Monceau, B. Pieraggi, Determination of Parabolic Rate Constants from a Local Analysis of Mass-Gain Curves, Oxidation of Metals 50 (1998) 477-493. https://doi.org/10.1023/A:1018860909826
[20] A. Chyrkin, R. Pillai, T. Galiullin, E. Wessel, D. Grüner, W.J. Quadakkers, External α-Al 2 O 3 scale on Ni-base alloy 602 CA. – Part I: Formation and long-term stability, Corrosion Science 124 (2017) 138-149. https://doi.org/10.1016/j.corsci.2017.05.017
[21] D. Samelor, L. Baggetto, R. Laloo, V. Turq, T. Duguet, D. Monceau, C. Vahlas, Amorphous Alumina Films Efficiently Protect Ti6242S against Oxidation and Allow Operation above 600 °C, Materials Science Forum 941 (2018) 1846-1852. https://doi.org/10.4028/www.scientific.net/MSF.941.1846
[22] T. Sanviemvongsak, PhD Thesis, INPT Toulouse, France (2020).
[23] A. Casadebaigt, PhD Thesis, INPT Toulouse, France (2020).
[24] M.W. Brumm, H.J. Grabke, The oxidation behaviour of NiAl - I. Phase transformations in the alumina scale during oxidation of NiAl and NiAl-Cr alloys, Corrosion Science 33 (1992) 1677-1690. https://doi.org/10.1016/0010-938X(92)90002-K
[25] X. Huang, L. Martinelli, S. Bosonnet, P.C.M. Fossati, L. Latu-Romain, Y. Wouters, Effect of Temperature on the Oxidation Mechanism of Ni-30Cr Alloy, Oxidation of Metals 96 (2021) 69-80. https://doi.org/10.1007/s11085-021-10049-4

[26] S. Sacré, U. Wienstroth, H.-G. Feller, L.K. Thomas, Influence of the phase compositions on the transient-stage high-temperature oxidation behaviour of an NiCoCrAlY coating material, Journal of Materials Science 28 (1993) 1843-1848. https://doi.org/10.1007/BF00595756
[27] R. Peraldi, D. Monceau, B. Pieraggi, Correlations between growth kinetics and microstructure for scales formed by high-temperature oxidation of pure nickel. II. Growth kinetics, Oxidation of Metals 58 (2002) 275-295. https://doi.org/10.1023/A:1020102604090
[28] G.C. Rybicki, J. Smialek, Effect of the tetha-alpha-Al2O3 transformation on the oxidation behavior of beta-NiAl+Zr, Oxidation of Metals 31 (1989) 275-304. https://doi.org/10.1007/BF00846690
[29] L. Bataillou, L. Martinelli, C. Desgranges, S. Bosonnet, K. Ginestar, F. Miserque, Y. Wouters, L. Latu-Romain, A. Pugliara, A. Proietti, D. Monceau, Growth Kinetics and Characterization of Chromia Scales Formed on Ni–30Cr Alloy in Impure Argon at 700 °C, Oxidation of Metals 93 (2020) 329-353. https://doi.org/10.1007/s11085-020-09958-7
[30] M.W. Brumm, H.J. Grabke, The oxidation behaviour of NiAl - II. Cavity formation beneath the oxide scale on NiAl of different stoichiometries, Corrosion Science 34 (1993) 547. https://doi.org/10.1016/0010-938X(93)90271-H
[31] B.A. Pint, Progress in understanding the reactive element effect since the Whittle and Stringer literature review, Proc. John Stringer Symposium on High Temperature Corrosion (2001) 9-19.
[32] S. Ford, R. Kartono, D.J. Young, Oxidation resistance of Pt-modified [gamma]/[gamma]' Ni-Al at 1150 °C, Surface and Coatings Technology 204 (2010) 2051-2054. https://doi.org/10.1016/j.surfcoat.2009.08.027
[33] E.E. Sileo, M. Jobbágy, C.O. Paiva-Santos, A.E. Regazzoni, Thermal Decomposition of Crystalline $Ni^{II}-Cr^{III}$ Layered Double Hydroxide: A Structural Study of the Segregation Process, The Journal of Physical Chemistry B 109 (2005) 10137-10141. https://doi.org/10.1021/jp050639v
[34] J.N. Roelofsen, R.C. Peterson, M. Raudsepp, Structural variation in nickel aluminate spinel (NiAl2O4), American Mineralogist 77 (1992) 522-528.
[35] L. Huang, X.F. Sun, H.R. Guan, Z.Q. Hu, Oxidation Behavior of a Single-Crystal Ni-base Superalloy in Air at 900, 1000 and 1100°C, Oxidation of Metals 65 (2006) 207-222. https://doi.org/10.1007/s11085-006-9016-z
[36] A. Sato, Y.L. Chiu, R.C. Reed, Oxidation of nickel-based single-crystal superalloys for industrial gas turbine applications, Acta Materialia 59 (2011) 225-240. https://doi.org/10.1016/j.actamat.2010.09.027
[37] U.R. Evans, The laws of expanding circles and spheres in relation to the lateral growth of surface films and the grain-size of metals, Transactions of the Faraday Society 41 (1945) 365-374. https://doi.org/10.1039/TF9454100365
[38] S. Taniguchi, Discussions on some Properties of Alumina Scales and their Protectiveness, Materials Science Forum 696 (2011) 51-56. https://doi.org/10.4028/www.scientific.net/MSF.696.51
[39] T.L. Barth, E.A. Marquis, Effects of Minor Alloying Elements on Alumina Transformation During the Transient Oxidation of β-NiAl, Oxidation of Metals 95 (2021) 293-309. https://doi.org/10.1007/s11085-021-10024-z

Table 1. Chemical composition of AM1 in ppm for Hf and S and in % for other elements (data provided by Safran Aircraft Engine).

		Ni	Ta	Cr	Co	W	Al	Mo	Ti	Hf (ppm)	S (ppm)
AM1	**wt%**	Bal.	7.97	7.54	6.61	5.49	5.2	2.01	1.2	460-490	0.104-0.123
	at%	Bal.	2.65	8.74	6.76	1.80	11.61	1.26	1.51	155-165	0.195-0.231

Table 2. Temperature and duration of the different dwells of the SMT-TGA experiment

Temperature (°C)	750	850	900	950	1000	1050	1100	1150	1200	1300	1100	1050
Time (h)	20	100	80	40	20	10	5	3	2	1	12	34

Table 3. Thicknesses of the different oxide sub-layers as determined by image analysis.

Thickness (µm)	20 h at 950°C	190 h at 950°C	10 min at 1100°C	140 h at 1100°C
Al_2O_3	0.56	0.8	0.36	1.39
Spinel	0.67	1.07	0.82	0.6
Rutile	0.49	0.37	0.12	0.22
NiO	0.03	0.23	0.19	/
Total	1.75	2.47	1.49	2.21

Table 4 Percentage of uncertainty of the three kinetic parameters of the model.

Parameters	**k_{p1}**		**k_{p2}**		**k_t**	
Percentage of uncertainty	+35%	-19%	+29%	-36%	+173%	-55%

Graphical abtsract

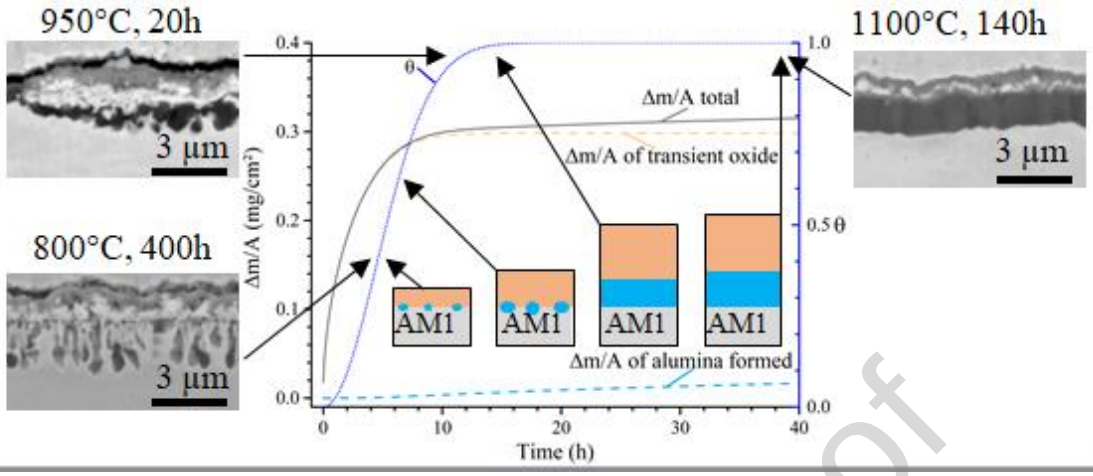

Author statement

Thomas Perez: Investigation, Methodology, Formal analysis, Writing – original draft. **Daniel Monceau:** Methodology, Supervision, Validation, Writing – review & editing, Project administration. **Clara Desgranges:** Resources, Funding acquisition, Supervision, Formal analysis, Writing – review & editing.

Declaration of interests

☒The authors declare that they have no known competing financial interests or personal relationships that could have appeared to influence the work reported in this paper.

☐The authors declare the following financial interests/personal relationships which may be considered as potential competing interests:

Highlights

- The oxidation behavior of AM1 superalloy was studied over the range 750 to 1300°C.
- Thermogravimetric analyses showed the existence of a kinetic transient regime.
- At short time and low temperature, AM1 is not an alumina-forming alloy.
- A model was developed to predict oxidation kinetics of AM1 for all temperatures.
- Kinetics from transient oxides growth to protective alumina was modeled.